



# Exceptional visible-light activities of g-C<sub>3</sub>N<sub>4</sub> nanosheets dependent on the unexpected synergistic effects of prolonging charge lifetime and catalyzing H<sub>2</sub> evolution with H<sub>2</sub>O



Xuliang Zhang, Xinxin Zhang, Jiadong Li, Jianhui Sun\*, Ji Bian, Jinshuang Wang, Yang Qu, Rui Yan, Chuanli Qin\*, Liqiang Jing\*

Key Laboratory of Functional Inorganic Material Chemistry (Heilongjiang University), Ministry of Education, School of Chemistry and Materials Science, International Joint Research Center for Catalytic Technology, Harbin, 150080, PR China

## ARTICLE INFO

### Keywords:

g-C<sub>3</sub>N<sub>4</sub> Nanosheet  
Charge lifetime prolonging  
Metallic synergistic effect  
Visible-light photocatalysis  
H<sub>2</sub> evolution

## ABSTRACT

It is highly desired to develop an efficient g-C<sub>3</sub>N<sub>4</sub>-based photocatalyst for energy production under visible-light irradiation. Herein, it is shown that the optimized g-C<sub>3</sub>N<sub>4</sub> nanosheet-based photocatalyst could exhibit exceptional photocatalytic activities for H<sub>2</sub> evolution under visible-light irradiation, by ~14-time improvement compared to that of bare g-C<sub>3</sub>N<sub>4</sub> one. It is confirmed by the methods of transient-state surface photovoltage responses, transient-state PL spectra and electrochemical measurements that the exceptional photocatalytic activities are attributed to the unexpected synergistic effects of prolonging the charge lifetime and catalyzing H<sub>2</sub> evolution by coupling nanocrystalline anatase TiO<sub>2</sub> as a proper-energy platform to accept visible-light-excited electrons from g-C<sub>3</sub>N<sub>4</sub> and by decorating a nano-sized noble metal as the co-catalyst respectively. Among three decorated noble metals (Ag, Au and Pt), to prolong the photogenerated charge lifetime is much meaningful for the used noble metal cocatalyst with weak catalytic function like Ag in H<sub>2</sub> evolution. Using nanocrystalline SnO<sub>2</sub> to replace TiO<sub>2</sub> is also applicable for the synergistic effect. Moreover, it is clarified by the designed experiment on photocatalytic CO<sub>2</sub> conversion to CD<sub>4</sub> in the presence of methanol in D<sub>2</sub>O that the resource of evolved H<sub>2</sub> is mainly from the adsorbed H<sub>2</sub>O other than the disassociated H<sup>+</sup> from methanol.

## 1. Introduction

Hydrogen is abundant in our environment and widely stored in water (H<sub>2</sub>O), hydrocarbons (such as methane, CH<sub>4</sub>), and other organics [1–4]. One of the challenges on using H<sub>2</sub> as a fuel comes from efficiently extracting it from these compounds. Photocatalytic technique provides a promising way to produce H<sub>2</sub> fuel by utilizing solar energy [5–9]. Especially, visible-light-driven photocatalysts are attractive since they can utilize the visible-light as the main part of solar energy (46%) [10]. Among various narrow-bandgap photocatalysts investigated in recent years, graphitic carbon nitride (g-C<sub>3</sub>N<sub>4</sub>) has drawn tremendous scientific attention for photocatalytic H<sub>2</sub> evolution due to its several advantages of visible-light absorption, cheapness, high chemical and thermal stability, suitable valence band (VB) and conduction band (CB) position [11,12]. Notably, its CB bottom is rather negative (-1.3 eV vs NHE) so that its photogenerated electrons would possess enough energy to induce the reduction reactions for H<sub>2</sub> evolution thermodynamically [13,14]. However, the photocatalytic activity of g-C<sub>3</sub>N<sub>4</sub> is still too low

to support its practical applications. This is usually attributed to the fast recombination of photogenerated electron-hole pairs and the lack of catalytic functions of separated electrons [15,16]. Thus, it is highly desired to develop a feasible method to enhance the separation of photogenerated charges and to provide strong catalytic functions for efficient visible-light photocatalysis on g-C<sub>3</sub>N<sub>4</sub> to produce H<sub>2</sub>.

Several attempts have been explored to enhance the charge separation of g-C<sub>3</sub>N<sub>4</sub>, including to construct a novel nanostructure, to couple another semiconductor and to decorate a noble metal, especially for the late ones [17–19]. Over the years, coupling a wide bandgap oxide, such as TiO<sub>2</sub> and SnO<sub>2</sub>, to improve the H<sub>2</sub> evolution activity of g-C<sub>3</sub>N<sub>4</sub> has been widely researched [14,20]. It is well accepted that the improved photoactivities are attributed to the promoted charge transfer so as to greatly prolong the charge lifetime. However, the apparent photoactivity is still unsatisfactory. This is because of the lack of catalytic functions for the transferred electrons to induce reduction reactions. Besides, another effective strategy is to only decorate a noble metal such as Pt, Au and Ag on the surface of g-C<sub>3</sub>N<sub>4</sub> [21–23]. In this

\* Corresponding authors.

E-mail addresses: [qinchuanli@hlju.edu.cn](mailto:qinchuanli@hlju.edu.cn) (C. Qin), [jinglq@hlju.edu.cn](mailto:jinglq@hlju.edu.cn) (L. Jing).

case, the modified noble metal could accept the photogenerated electrons so as to prolong the charge lifetime, simultaneously acting as the co-catalyst to provide the catalytic function for electron-induced reduction reactions. This is well responsible for the obviously improved photocatalytic activities of g-C<sub>3</sub>N<sub>4</sub> for H<sub>2</sub> evolution after decorating a noble metal. By comparison, it is naturally deduced that to modify with a noble metal is much feasible for efficient photocatalysis on g-C<sub>3</sub>N<sub>4</sub> compared with a wide bandgap oxide.

As for the modified noble metal, it is understandable that it could accept the photogenerated electrons from g-C<sub>3</sub>N<sub>4</sub> since it possesses a rather low Fermi energy level. However, it is not quite beneficial to prolong the lifetime of transferred electrons with enough thermodynamic energy. This would make the photoactivity improvement to be limited to a certain degree, and it is different for different noble metals [24]. However, those are usually neglected since seldom related works have been reported to date. In addition, it should be pointed out that it is much favorable for the transferred electrons with enough thermodynamic energy to prolong the charge lifetime of g-C<sub>3</sub>N<sub>4</sub> by coupling a wide bandgap oxide like TiO<sub>2</sub>. Naturally expected, this will facilitate the transferred electrons to initiate the reduction reactions if a noble metal is used as the cocatalyst. Thus, it is assumed that there is a synergistic effect of prolonging the proper-energy electron lifetime and providing the catalytic functions to evolve H<sub>2</sub> on efficient photocatalysis of g-C<sub>3</sub>N<sub>4</sub>. Obviously, it is much meaningful to clarify the assumption for developing a highly efficient g-C<sub>3</sub>N<sub>4</sub>-based photocatalyst to produce solar fuels.

Based on the above consideration, it is much feasible to improve the visible-light photocatalytic activity of g-C<sub>3</sub>N<sub>4</sub> by simultaneously coupling a wide bandgap oxide and decorating a noble metal. For the coupled oxide, anatase TiO<sub>2</sub> is chosen as the model semiconductor for it is a widely-used wide bandgap oxide, and its CB position is in proper energy level for H<sub>2</sub> evolution from water [25–27]. It is interesting to choose Ag as a model cocatalyst because it is a cheaper noble metal compared with Pt and Au, along with relative comparison investigation [28,29]. Moreover, it is necessary to deeply explore the photogenerated charge transfer and lifetime by employing different time-resolved photo-physical techniques like surface photovoltage response and photoluminescence (PL) spectra [25,30,31]. In addition, it is widely accepted that methanol is always used as the sacrificial agent to capture holes for efficiently photocatalytic H<sub>2</sub> evolution, simultaneously providing H<sup>+</sup> [32,33]. Thermodynamically, it seems that it is much favorable for the disassociated H<sup>+</sup> to evolve H<sub>2</sub> by photocatalysis, and some works suggest that the H<sup>+</sup> provided by methanol oxidation will participate in the H<sub>2</sub> evolution process [33–35]. However, it is still disagreeable that the evolved H<sub>2</sub> mainly comes from the used H<sub>2</sub>O or from the H<sup>+</sup> provided by the methanol oxidation. Therefore, it is much meaningful to clarify the mentioned-above points from the scientific point of view in photocatalysis for energy production.

Herein, g-C<sub>3</sub>N<sub>4</sub> nanosheet was firstly synthesized by the method of calcining urea, and then modified by coupling anatase-phase TiO<sub>2</sub> through a wet-chemical process and then by decorating a noble metal via a photodeposition method. It is shown that the optimized g-C<sub>3</sub>N<sub>4</sub> nanosheet-based photocatalysts could exhibit exceptional photocatalytic activities for H<sub>2</sub> evolution under visible-light irradiation. It is confirmed that the exceptional photocatalytic activities are attributed to the usually-neglected synergistic effects of prolonging the charge lifetime and catalyzing H<sub>2</sub> evolution. Among the three used noble metals, the synergistic effect with the coupled TiO<sub>2</sub> for used Ag is much obvious, compared to those for Au and Pt, indicating that prolonging the photogenerated electron lifetime is much meaningful for the used Ag with weak catalytic function. Moreover, the designed D<sub>2</sub>O isotope experiment for photocatalytic CO<sub>2</sub> conversion to CD<sub>4</sub> means that the evolved H<sub>2</sub> mainly originates from the adsorbed H<sub>2</sub>O other than the disassociated H<sup>+</sup> from methanol. This work provides a new physical insight on developing an efficient g-C<sub>3</sub>N<sub>4</sub>-based photocatalyst for energy production.

## 2. Experimental section

All the chemicals were of analytical grade and used as-received without further purification. Deionized water was used throughout the experiments.

### 2.1. Synthesis of g-C<sub>3</sub>N<sub>4</sub>

To prepare g-C<sub>3</sub>N<sub>4</sub>, in a typical process, 30 g of urea was taken and grinded into fine powder. Then the powder was transferred to a 100 mL aluminum crucible and treated in a muffle furnace at 550 °C (temp ramp 0.5 °C/min) for 3 h. After cooling to room temperature naturally, the product was grinded into fine powder prior to characterization.

### 2.2. Synthesis of TiO<sub>2</sub> nanoparticles

A sol-hydro-thermal method was employed to synthesize TiO<sub>2</sub> nanoparticles: 5 mL Ti(OBu)<sub>4</sub> was dissolved in 5 mL anhydrous ethanol, the solution was stirred for 30 min, denoted as solution A. 20 mL anhydrous ethanol, 5 mL water and 1 mL 70% HNO<sub>3</sub> were taken, then mixed and stirred for 30 min, denoted as solution B. Then solution A was added to solution B in a dropwise way under vigorous stirring condition at room temperature, and a yellowish transparent sol was obtained. Subsequently, 30.85 mL of the as-prepared solution was transferred into a Teflon-lined stainless steel autoclave and hydrothermally treated at 160 °C for 6 h. After cooling to room temperature naturally, the sample was centrifuged and washed three times with deionized water followed by absolute ethanol, and finally dried in air at 80 °C to obtain the TiO<sub>2</sub> precursor. TiO<sub>2</sub> nanoparticles were obtained by further treating TiO<sub>2</sub> precursor in a muffle furnace at 450 °C (temp ramp 10 °C/min) for 2 h.

### 2.3. Synthesis of TiO<sub>2</sub> coupled g-C<sub>3</sub>N<sub>4</sub>

1 g of the freshly prepared g-C<sub>3</sub>N<sub>4</sub> was dispersed into a mixed solvent of 25 mL ethanol and 25 mL deionized water. Then different amounts (20, 40, 60 and 80 mg) of TiO<sub>2</sub> precursor were added into the solution and kept under vigorous stirring for 2 h. Then the samples were dried at 80 °C in the water bath under vigorous stirring. Finally, the samples were annealed at 450 °C (temp ramp 10 °C/min) for 2 h. The samples were denoted as xT/g-C<sub>3</sub>N<sub>4</sub>, in which the x indicates the mass ratio percentage of TiO<sub>2</sub> precursor to g-C<sub>3</sub>N<sub>4</sub> in theory.

### 2.4. Synthesis of SnO<sub>2</sub> nanoparticles

SnO<sub>2</sub> was prepared by a hydrothermal method. In a typical process, 0.561 g SnCl<sub>4</sub>·5H<sub>2</sub>O was dissolved in 10 mL deionized water under continuous stirring for 1 h, denoted as solution A. 1.95 g sodium oleate (C<sub>18</sub>H<sub>33</sub>NaO<sub>2</sub>) was dissolved in 10 mL deionized water and 20 mL acetic acid under continuous stirring for 1 h, denoted as solution B. The solution A was added dropwise into solution B, and the resulting emulsion was stirred for another 1 h. Finally, 30 mL of the emulsion was kept at 180 °C for 24 h in a Teflon-lined stainless-steel vessel and then cooled naturally to room temperature. Then the emulsion sequentially was washed with deionized water and absolute ethanol, followed by drying it at 80 °C in air to get SnO<sub>2</sub> precursor.

### 2.5. Synthesis of SnO<sub>2</sub> coupled g-C<sub>3</sub>N<sub>4</sub>

1 g of the freshly prepared g-C<sub>3</sub>N<sub>4</sub> was dispersed into a mixed solvent of 25 mL ethanol and 25 mL deionized water. Then 60 mg SnO<sub>2</sub> precursor was added into the solution and kept under vigorous stirring for 2 h. Then the sample was dried at 80 °C in the water bath under vigorous stirring. Finally, the sample was annealed at 450 °C (temp ramp 10 °C/min) for 2 h.

## 2.6. Photodeposition of Ag nanoparticles

In a typical experiment, different amounts (the theoretical mole ratios of Ag to g-C<sub>3</sub>N<sub>4</sub> were 0.1, 0.25, 0.4 and 0.5:100) of Ag nanoparticles were deposited on the g-C<sub>3</sub>N<sub>4</sub> surface by the photo-deposition method. In the first step, the desired amount of silver nitrate (AgNO<sub>3</sub>) and 1 g g-C<sub>3</sub>N<sub>4</sub> were dispersed in a mixed solution of 50 mL methanol and 100 mL deionized water in a 250 mL beaker covered with a sealing film. Then the samples were treated by turns of sonication and stir, each for 10 min. After that, nitrogen gas was bubbled through the samples for 1 h to generate an inert atmosphere for the photodeposition of Ag nanoparticles. And then irradiated under a 300 W xenon lamp with a 420 nm cut-off filter for 3 h, under vigorous stirring. Finally, the samples were centrifuged and washed for three times with deionized water followed by absolute ethanol, and finally dried in air at 80 °C. The samples were denoted as yAg/g-C<sub>3</sub>N<sub>4</sub>, in which y means the mole ratio percentage of added Ag to g-C<sub>3</sub>N<sub>4</sub> in theory. Particularly, to obtain g-C<sub>3</sub>N<sub>4</sub> co-modified with noble metal and TiO<sub>2</sub> or SnO<sub>2</sub>, the noble metal was photo deposited on TiO<sub>2</sub> or SnO<sub>2</sub> coupled g-C<sub>3</sub>N<sub>4</sub>.

## 2.7. Characterization

We took various techniques to characterize the prepared samples. The crystal structure was determined by of Bruker D8 Advance X-ray diffractometer equipped with graphite monochromatized Cu K $\alpha$  radiation with wave length equal to 1.54056 Å. For the X-ray diffraction measurement, the voltage was accelerated to 30 kV and the emission current was fixed at 20 mA. The UV-vis DRS spectra were collected using a Shimadzu UV-2550 spectrometer with BaSO<sub>4</sub> as the reference. Electron micrographs were taken by using a JEOL JEM-2010 transmission electron microscope operated at 200 kV. The elemental chemical states of the samples were examined by XPS using a Kratos-Axis Ultra DLD apparatus with an Al (mono) X-ray source and the binding energies of the samples were calibrated with respect to the signal for adventitious carbon (284.55 eV). The fourier transform infrared (FT-IR) spectra were collected using a Bruker Vector FT-IR spectrometer (6700) with a high-sensitivity micro-channel detector detector which was cooled by liquid N<sub>2</sub>. Transient-state PL (TS-PL) spectra were recorded with a single photon counting spectrometer from (Edinburgh Instrument, FLS 920) with 1 μs pulse lamp as the excitation. The steady-state PL spectra were measured with a PE LS 55 spectrofluoro-photometer at excitation wavelength of 390 nm.

The atmosphere-controlled SS-SPS measurement was carried out by using a home-built apparatus equipped with a lock-in amplifier (SR830) and synchronized with a light chopper (SR540). The sample was sandwiched between two indium tin oxide (ITO) glass electrodes and irradiated through a 500 W xenon lamp (CHF XQ500 W, Global xenon lamp power) to obtain a monochromatic light by passing through a double prism monochromator (SBP300). The transient-state surface photovoltage (TS-SPV) responses of the samples were measured in air atmosphere at room temperature. In a typical measurement, the sample chamber was connected to an ITO glass at the top electrode and a steel substrate at bottom electrode, and a thick mica spacer was placed between the ITO glass and the sample to decrease the space charge region at the ITO-sample interface. The samples were excited by a radiation pulse of 355 nm with 10 ns width from the second harmonic of a neodymium-doped yttrium aluminum garnet (Nd:YAG) laser (Lab-130-10H, Newport, Co.). The signals were amplified with a pre-amplifier and registered with a 1 GHz digital phosphor oscilloscope (DPO 4104B, Tektronix).

## 2.8. Electrochemical reduction measurement

The electrochemical reduction measurement in this work was operated using a traditional three-electrode system. The working electrode was a glassy carbon electrode of 0.3 cm in diameter. The

saturated calomel electrode was used as the reference electrode and a Pt sheet was used as the counter electrode. The electrolyte used in our test was 0.5 M NaClO<sub>4</sub>. First, 5 mg of different samples mixed with 20 μL of 5 wt % Nafion ionomer was dissolve in 0.18 mL ethanol aqueous solution. Then the catalyst ink was ultrasonicated for 30 min, and a suitable mass of the ink was dropped uniformly onto the clean GC electrode surface and then dried it in air. An AUTOLAB PG STAT101 electrochemical workstation was employed to test electrochemical activity. At the beginning, electrode potentials were cycled between two potential limits until perfectly overlapping, afterward we obtained the I-V curves. All the experiments were performed at room temperature.

## 2.9. Measurement of ·OH amount

In a typical measurement, 0.05 g of each sample was dispersed in a beaker containing 40 mL of 0.001 M coumarin solution. Prior to irradiation, the samples were stirred magnetically for 10 min to achieve adsorption-desorption equilibrium. The visible-light irradiation time for each sample was 1 h. After that, the sample was centrifuged and a certain amount of the pellucid liquid was taken and transferred in a Pyrex glass cell for the measurement of 7-hydroxycoumarin with characteristic emission peak at 460 nm through a spectrofluorometer (Perkin-Elmer LS55).

## 2.10. Evaluation of photocatalytic activity for H<sub>2</sub> evolution

The H<sub>2</sub> evolution was tested under visible-light ( $\lambda > 400$ ) to evaluate the photocatalytic activities of the samples. The experiments were performed in a 250 mL quartz cell. For each experiment, 0.1 g of the sample was put in a mixture of 80 mL deionized water and 20 mL of methanol (sacrificial agent). A 300 W xenon lamp was used as the visible-light irradiation source, and the sample was irradiated in a closed water circulating system for 4 h. The amount of evolved H<sub>2</sub> was detected with an online TCD gas chromatograph (Tech, GC-9700, nitrogen gas carrier). The stability and recyclability tests were measured for 30 h, with a 5-h run cycle. For each run, the sample was dried and irradiated under visible-light.

## 2.11. Evaluation of photocatalytic activity for CO<sub>2</sub> reduction

In the photocatalytic reduction of CO<sub>2</sub>, 0.2 g of the sample was dispersed in 8 mL water (with or without 2 mL methanol) and the solution was contained in a cylindrical steel reactor with 100 mL volume and 3.5 cm<sup>2</sup> area. Then high purity CO<sub>2</sub> gas was bubbled in the reactor after passing through water for reaching ambient pressure. Then the CO<sub>2</sub>/H<sub>2</sub>O system was equilibrated for 1 h and a 300 W xenon lamp was used as the light source with a cut-off filter of 420 nm for the photocatalytic reaction. After irradiation for 8 h, continually 0.5 mL of gas was taken from the reaction cell at given time interval for the analysis of CH<sub>4</sub> concentration using a gas chromatograph (GC-2014 with FID detector; Shimadzu Corp., Japan). A gas chromatography-mass spectrometer (MS5977A, America Aligent) was employed for the analysis of CD<sub>4</sub> concentration to perform the isotopic experiments about CO<sub>2</sub> reduction with H<sub>2</sub>O changed to D<sub>2</sub>O.

## 3. Results and discussion

### 3.1. Structural characterization

According to the X-ray diffraction (XRD) patterns (Fig. S1), it is confirmed that the peaks at  $2\theta = 13.1^\circ$  and  $27.4^\circ$  can be indexed to (100) and (002) diffraction planes of g-C<sub>3</sub>N<sub>4</sub> [36]. A new peak appears at  $2\theta = 25.2^\circ$  after coupling TiO<sub>2</sub> which belongs to anatase TiO<sub>2</sub> [37]. Moreover, two additional peaks appearing at  $2\theta = 38.1^\circ$  and  $44.2^\circ$  after decorating Ag can be indexed to (111) and (200) facets of Ag [38]. One can notice that the related XRD peaks become strong with increasing

the amount of Ag or  $\text{TiO}_2$ . Interestingly, the XRD pattern of 0.25 Ag/6 T/g-C<sub>3</sub>N<sub>4</sub> clearly demonstrates that metallic Ag and anatase  $\text{TiO}_2$  are successfully co-modified on g-C<sub>3</sub>N<sub>4</sub>. UV-vis DRS (Fig. S2) show that the bandgap of g-C<sub>3</sub>N<sub>4</sub> is hardly changed after coupling  $\text{TiO}_2$  and decorating Ag, while a neglectable optical absorption appears in the visible-light region presumably due to the plasmonic effect of nanosized Ag [39].

The surface composition and chemical state of the elements in the prepared samples are investigated by the X-ray photoelectron spectroscopy (XPS) (Fig. S3). For all samples, the typical peaks of C 1s and N 1s are in good agreement with the previous reports [40]. In particular, the peaks in XPS spectra of Ag 3d<sub>3/2</sub> and Ag 3d<sub>5/2</sub> are observed at 368.3 and 374.3 eV for 0.25 Ag/g-C<sub>3</sub>N<sub>4</sub> and 0.25 Ag/6 T/g-C<sub>3</sub>N<sub>4</sub> samples, indicating the existence of Ag<sup>0</sup> [41]. Moreover, the strong peaks of Ti 2p located at 458.5 (Ti 2p<sub>3/2</sub>) and 464.2 eV (Ti 2p<sub>1/2</sub>) and O 1s located at energy of 529.8 eV (the crystal lattice oxygen) are observed in the samples of 6 T/g-C<sub>3</sub>N<sub>4</sub> and 0.25 Ag/6 T/g-C<sub>3</sub>N<sub>4</sub> which means the existence of  $\text{TiO}_2$  [20,42]. In addition, one can see from the O 1s spectrum that the peak of the crystal lattice oxygen is not found in the Ag-decorated g-C<sub>3</sub>N<sub>4</sub>.

Transmission electron microscopy (TEM) images were taken to characterize the morphology and measure the size of the as-prepared hybrid structures. As seen in Figs. 1A and S4, the g-C<sub>3</sub>N<sub>4</sub> is sheet-like structure, the diameters of  $\text{TiO}_2$  and Ag nanoparticle are estimated to be ~5 nm and ~18 nm, respectively. It is noticed that the distances between the adjacent lattices are determined to be 0.352 and 0.236 nm, respectively, corresponding to the (101) plane of anatase  $\text{TiO}_2$  and the (111) plane of Ag [43,44]. Thus, anatase  $\text{TiO}_2$  and metallic Ag are successfully co-modified on g-C<sub>3</sub>N<sub>4</sub> with close contacts. This is in good agreement with the XRD results.

### 3.2. Photogenerated charge separation and lifetime

To investigate the photogenerated charge properties of the samples, the surface photovoltaic technique including steady-state surface photovoltaic spectroscopy (SS-SPS), TS-SPV responses and PL spectra were employed. In general, the stronger is the SS-SPS response, the higher is the charge separation. It is confirmed from the SS-SPS responses and PL spectra (Fig. S5 and S6A) that the photogenerated charge separation of g-C<sub>3</sub>N<sub>4</sub> could be enhanced a lot after coupling a proper amount of  $\text{TiO}_2$ , while enhanced a little after decorating a proper amount of Ag. Interestingly, the co-modified g-C<sub>3</sub>N<sub>4</sub> (0.25 Ag/6 T/g-C<sub>3</sub>N<sub>4</sub>) displays the rather strong SS-SPS response, indicating the much high photogenerated charge separation.

To compare the separation and lifetime of the photogenerated

charges, the TS-SPV responses of g-C<sub>3</sub>N<sub>4</sub>, 6 T/g-C<sub>3</sub>N<sub>4</sub>, 0.25 Ag/g-C<sub>3</sub>N<sub>4</sub> and 0.25 Ag/6 T/g-C<sub>3</sub>N<sub>4</sub> were measured to further reveal the photo-generated charge property. As shown in Fig. 1B, it is noted from the intensities of the TS-SPV responses that the charge separation situation is consistent with the SS-SPS results. Moreover, the quantitative study of carrier dynamics usually provides further understanding of photo-generated charge properties of the photocatalysts. One can see that the photovoltage signals quickly climb to the maximum in the photovoltage spectra [45]. Then, the spatially dependent recombination between the free charges and localized centers by the diffusion process obeys the logarithmic law [46]. As seen in the Fig. 1B, all the TS-SPV decay profiles are well fitted by an exponential function. According to the fitted time constants of different samples, it is confirmed that the charge lifetime of g-C<sub>3</sub>N<sub>4</sub> could be greatly prolonged after coupling  $\text{TiO}_2$ , while it is not obvious after decorating Ag. Notably, the fitted time constant of 1065  $\mu\text{s}$  in 0.25 Ag/6 T/g-C<sub>3</sub>N<sub>4</sub> is around ~100  $\mu\text{s}$  long compared to that of g-C<sub>3</sub>N<sub>4</sub>. In general, the long charge lifetime by the surface photovoltaic response corresponds to the efficient photogenerated charge separation.

Further measurements of the PL lifetimes are conducted to explore the charge transfer from the g-C<sub>3</sub>N<sub>4</sub> by TS-PL spectra. Fig. 2 shows the normalized TS-PL kinetics of g-C<sub>3</sub>N<sub>4</sub>, 6 T/g-C<sub>3</sub>N<sub>4</sub>, 0.25 A g/g-C<sub>3</sub>N<sub>4</sub> and 0.25 Ag/6 T/g-C<sub>3</sub>N<sub>4</sub>. The TS-PL decay profiles for g-C<sub>3</sub>N<sub>4</sub> were observed to have two distinct decay components: the initial fast decay over 1  $\mu\text{s}$ , and a slow decay over 10  $\mu\text{s}$ , in consistent with the recent reports [47]. As well known, the electron transfer from g-C<sub>3</sub>N<sub>4</sub> to  $\text{TiO}_2$  or Ag is energetically favorable. From the decay curves (Fig. 2 and Table. S1), it is shown that the decay lifetime of g-C<sub>3</sub>N<sub>4</sub> is decreased after coupling  $\text{TiO}_2$  or after decorating Ag, and it is much obvious for the coupled  $\text{TiO}_2$ . The shortened PL decays mean that the electron transfer adds another decay channel to the excited states of g-C<sub>3</sub>N<sub>4</sub>, in consistent with our considerations that the photogenerated charge separation of g-C<sub>3</sub>N<sub>4</sub> could be enhanced after modifying with a proper amount of Ag and  $\text{TiO}_2$ . In this case, the photogenerated electrons in g-C<sub>3</sub>N<sub>4</sub> can be timely extracted, thus lowering the fast recombination. This is in good agreement with the TS-SPV results for the lowered fast recombination will provide more electrons to participate in generating the TS-SPV signal.

It is generally accepted that the amount of produced hydroxyl radicals ( $\cdot\text{OH}$ ) can reflect the separation of photogenerated charges in the photocatalytic process [48]. Thus, it is meaningful to test the  $\cdot\text{OH}$  amount to further verify the charge separation in a photochemical sense. Since the coumarin easily reacts with  $\cdot\text{OH}$  to produce luminescent 7-hydroxy-coumarin, the coumarin fluorescent method is often utilized to measure the  $\cdot\text{OH}$  amount. The fluorescence intensity related to the amounts of produced  $\cdot\text{OH}$  for different C<sub>3</sub>N<sub>4</sub>-based samples are

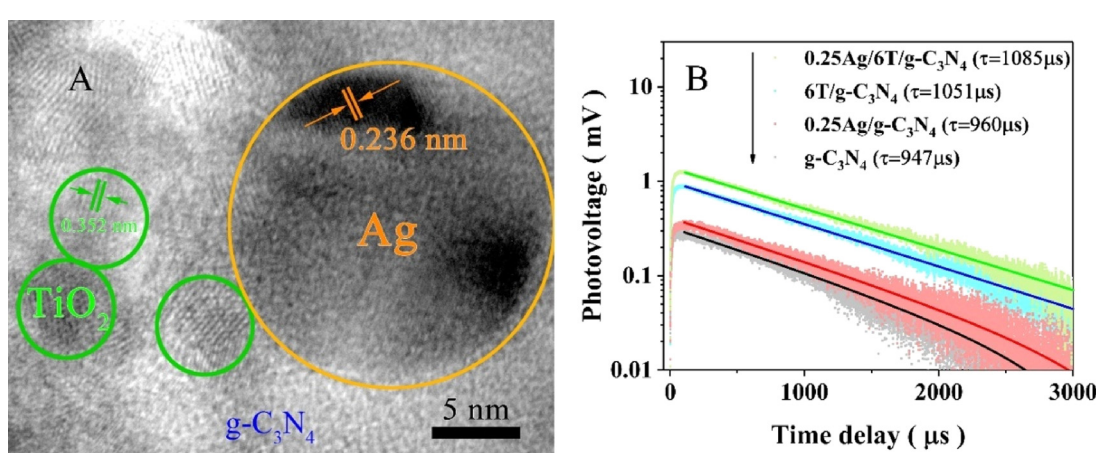


**Fig. 1.** High-resolution transmission electron microscopy (HRTEM) image of 0.25 Ag/6 T/g-C<sub>3</sub>N<sub>4</sub> sample (A). Transient-state surface photovoltaic (TS-SPV) responses of g-C<sub>3</sub>N<sub>4</sub>, 0.25 A g/g-C<sub>3</sub>N<sub>4</sub>, 6 T/g-C<sub>3</sub>N<sub>4</sub> and 0.25 Ag/6 T/g-C<sub>3</sub>N<sub>4</sub> samples (B). xT/g-C<sub>3</sub>N<sub>4</sub> means  $\text{TiO}_2$  coupled g-C<sub>3</sub>N<sub>4</sub> in which x is the mass ratio percentage of  $\text{TiO}_2$  to g-C<sub>3</sub>N<sub>4</sub> in theory. yAg/g-C<sub>3</sub>N<sub>4</sub> means Ag decorated g-C<sub>3</sub>N<sub>4</sub> in theory.

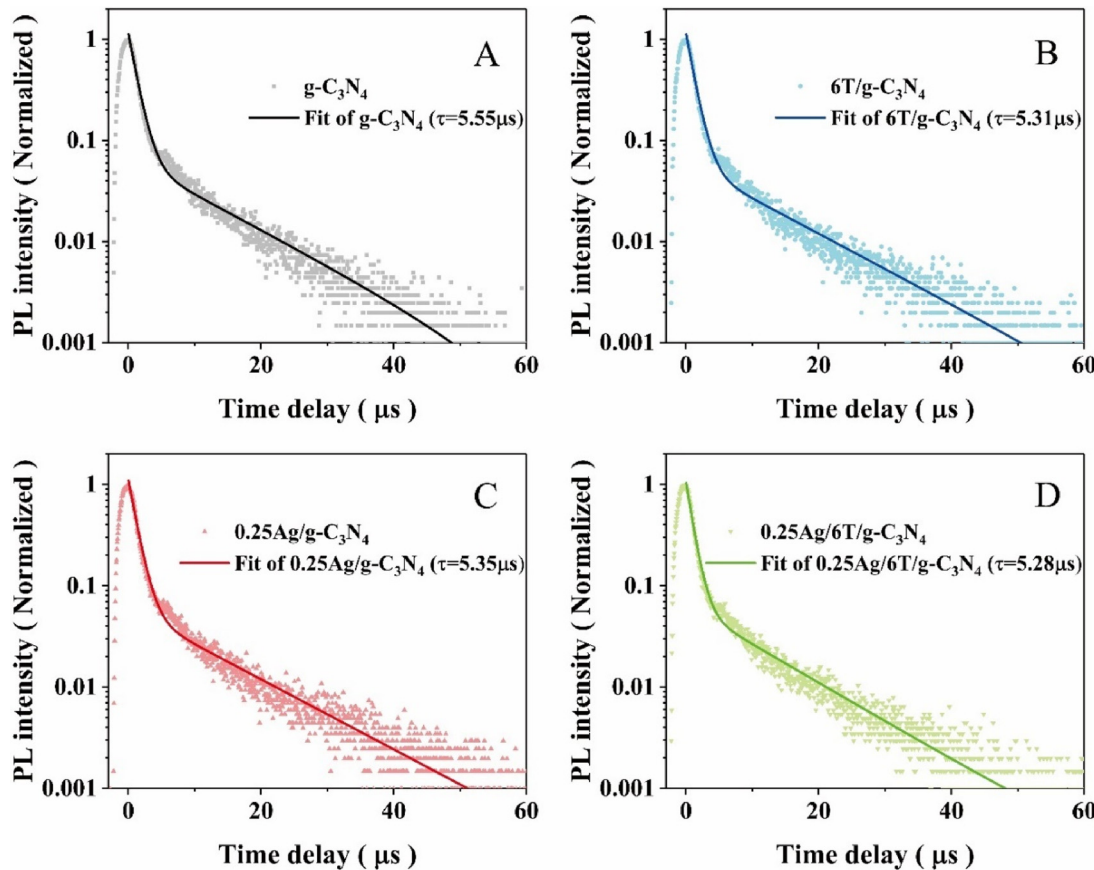


Fig. 2. Transient-state photoluminescence spectra of g-C<sub>3</sub>N<sub>4</sub>, 0.25 A g/g-C<sub>3</sub>N<sub>4</sub>, 6 T/g-C<sub>3</sub>N<sub>4</sub> and 0.25 A g/6 T/g-C<sub>3</sub>N<sub>4</sub> samples with 420 nm laser excitation.

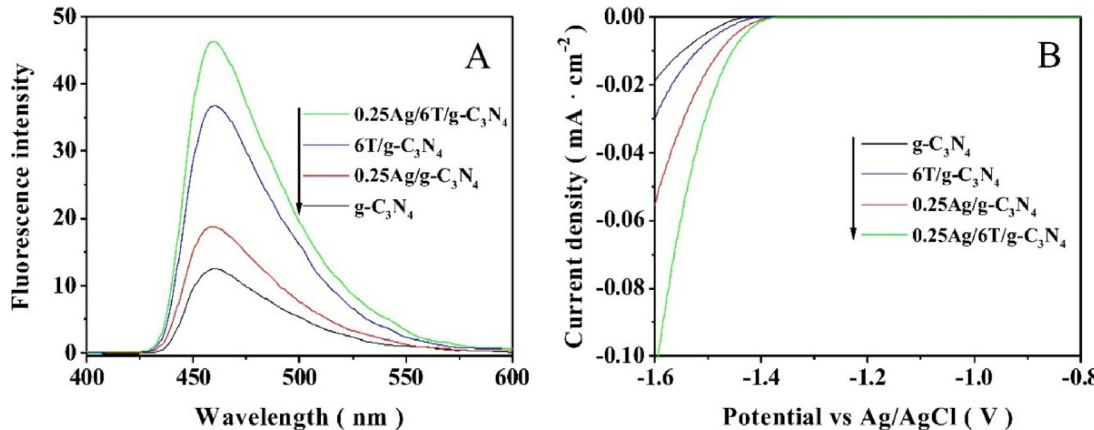


Fig. 3. Hydroxyl radical amount-related fluorescence spectra (A) and electrochemical I–V curves in the N<sub>2</sub> atmosphere (B) of g-C<sub>3</sub>N<sub>4</sub>, 0.25 A g/g-C<sub>3</sub>N<sub>4</sub>, 6 T/g-C<sub>3</sub>N<sub>4</sub> and 0.25 A g/6 T/g-C<sub>3</sub>N<sub>4</sub> samples.

shown in Fig. 3A. As expected, one can see that the observed fluorescence intensity order is as follows: g-C<sub>3</sub>N<sub>4</sub> < 0.25 Ag/g-C<sub>3</sub>N<sub>4</sub> < 6 T/g-C<sub>3</sub>N<sub>4</sub> < 0.25 Ag/6 T/g-C<sub>3</sub>N<sub>4</sub>, which is well agreeable with the above photophysical results. Therefore, it is clearly demonstrated that the separation and lifetime of photogenerated charges on g-C<sub>3</sub>N<sub>4</sub> are increased after coupling anatase TiO<sub>2</sub> and decorating metallic Ag, and it is much obvious for the coupled TiO<sub>2</sub> compared for the decorated Ag. Interestingly, the separation and lifetime of photogenerated charges on g-C<sub>3</sub>N<sub>4</sub> could be increased greatly after co-modifying TiO<sub>2</sub> and Ag.

### 3.3. Evaluation of photocatalytic activities

To compare the catalytic property for H<sub>2</sub> evolution, electrochemical

reduction curves were recorded (Fig. 3B). The observed cathode current in the range of -1.6 V to -1.3 V versus Ag/AgCl is attributed to the water reduction for H<sub>2</sub> evolution [49,50]. It is shown that 6 T/g-C<sub>3</sub>N<sub>4</sub> and 0.25 Ag/g-C<sub>3</sub>N<sub>4</sub> are favorable for electrochemical H<sub>2</sub> evolution compared with g-C<sub>3</sub>N<sub>4</sub>, while it is much marked for 0.25 Ag/g-C<sub>3</sub>N<sub>4</sub>. In particular, the catalytic property of co-modified g-C<sub>3</sub>N<sub>4</sub> is the best, indicating that it is much beneficial for water reduction.

As seen from the photocatalytic data (Fig. S7), the visible-light photocatalytic activity of g-C<sub>3</sub>N<sub>4</sub> for H<sub>2</sub> evolution in the presence of methanol is improved after coupling a proper amount of TiO<sub>2</sub> and decorating a proper amount of Ag, respectively, and it is much obvious for the resulting 6 T/g-C<sub>3</sub>N<sub>4</sub> and 0.25 Ag/g-C<sub>3</sub>N<sub>4</sub>. Unexpectedly, the photoactivity of 0.25 Ag/g-C<sub>3</sub>N<sub>4</sub> is higher than that of 6 T/g-C<sub>3</sub>N<sub>4</sub>,

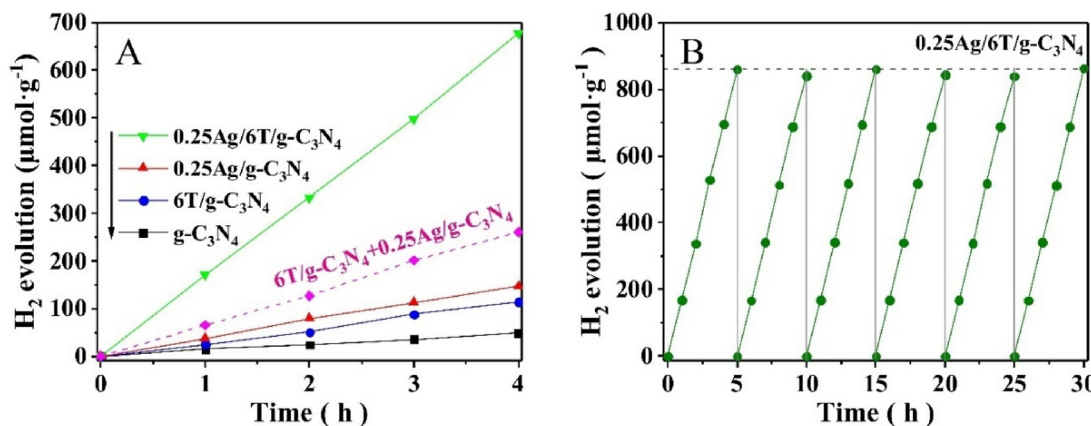


**Fig. 4.** Visible-light photocatalytic activities for  $H_2$  evolution on  $g\text{-}C_3N_4$ ,  $0.25\text{ Ag/g-C}_3N_4$ ,  $6\text{ T/g-C}_3N_4$  and  $0.25\text{ Ag/6 T/g-C}_3N_4$  samples (A). Stability test of  $0.25\text{ Ag/g-C}_3N_4$  during the photocatalytic  $H_2$  evolution for 30 h (B).

which is consistent with the catalytic property for  $H_2$  evolution, while different from the photogenerated charge separation and lifetime. This illustrates that it is much important for efficient photocatalysis on  $g\text{-}C_3N_4$  to improve the catalytic property for  $H_2$  evolution compared to increase the photogenerated charge separation and lifetime. Interestingly, the visible-light photoactivity of  $0.25\text{ Ag/6 T/g-C}_3N_4$  exhibits boost improvement as compared to bare  $g\text{-}C_3N_4$  (Fig. 4A), even much higher than the sum of  $6\text{ T/g-C}_3N_4$  and  $0.25\text{ Ag/g-C}_3N_4$ . This clearly reveals that there is an unexpected synergistic effect of prolonging the charge lifetime and providing the catalytic function for efficiently photocatalytic  $H_2$  evolution on  $g\text{-}C_3N_4$ . In addition, the quantum efficiency of  $0.25\text{ Ag/6 T/g-C}_3N_4$  under the single-wavelength (420 nm) irradiation is 1.73% which is much higher than the pure  $g\text{-}C_3N_4$  (0.30%) (Supporting Information), and the photocatalytic recyclable test of  $0.25\text{ Ag/6 T/g-C}_3N_4$  for 6 runs during the photocatalytic  $H_2$  evolution (Fig. 4B) reveals that it is stable.

#### 3.4. Discussion on mechanism

Based on the above results, it is indicated that the main role of the coupled  $TiO_2$  as the new energy platform is to prolong the lifetime of photogenerated electrons with proper thermodynamic energy of  $g\text{-}C_3N_4$ , consequently leading to the enhanced charge separation, while the decorated Ag mainly works as a cocatalyst to improve the catalytic capability for  $H_2$  evolution. Hence, it is believable that the synergistic effect of prolonging the charge lifetime and providing the catalytic function is well responsible for the exceptional visible-light photocatalytic activity of  $0.25\text{ Ag/6 T/g-C}_3N_4$  for  $H_2$  evolution. Similar to the coupled  $TiO_2$ , the decorated Ag could also accept the photogenerated electrons of  $g\text{-}C_3N_4$  so as to enhance the charge separation. However, the effect on the charge separation is weak for the decorated Ag compared with the coupled  $TiO_2$  based on the above photophysical and photochemical results. This is possibly attributed to the low Fermi energy of Ag so that the transferred electrons possess low thermodynamic energy. Further, it would not be favorable for the transferred electrons to induce reduction reactions for  $H_2$  evolution, even at the aid of catalytic function.

To further confirm the above points, we have carried out similar investigations by replacing Ag with Au and Pt. By means of XRD patterns and XPS spectra, it is confirmed that the metallic Au and Pt with the same amount as Ag are employed to modify  $g\text{-}C_3N_4$  (Figs. S8A, S8B, S9A and S9B) [3,22,23,51]. Likewise, one can see from the UV-vis DRS results that the bandgap of  $g\text{-}C_3N_4$  is almost unchanged after coupling  $TiO_2$  and decorating Au or Pt (Figs. S8C and S9C). As shown from the SS-SPS, PL and TS-SPV results (Figs. S6B, S6C, S8D, S8E, S9D, S9E and Table 1), it is confirmed that the charge separation is increased and the charge lifetime is prolonged after decorating Au or Pt. As expected, it is

**Table 1**

TS-SPV lifetimes ( $\tau_{TPV}$ ), average transient-state PL lifetimes ( $\tau_{PL}$ ) and rates of evolved  $H_2$  by visible-light photocatalysis on different samples ( $R_{H2}$ ), along with the rate ratios of evolved  $H_2$  on metal/ $TiO_2/g\text{-}C_3N_4$  to on  $TiO_2/g\text{-}C_3N_4$  (RR).

Different samples	$\tau_{TPV}$ (μs)	$\tau_{PL}$ (μs)	$R_{H2}$ ( $\mu\text{mol}\cdot\text{g}^{-1}\cdot\text{h}^{-1}$ )	RR
$g\text{-}C_3N_4$	947	5.55	12.15	
$6\text{ T/g-C}_3N_4$	1051	5.31	28.38	
$0.25\text{ Ag/g-C}_3N_4$	960	5.35	36.79	4.6
$0.25\text{ Ag/6 T/g-C}_3N_4$	1085	5.28	169.46	
$0.25\text{ Au/g-C}_3N_4$	971	5.19	80.37	2.7
$0.25\text{ Au/6 T/g-C}_3N_4$	1116	5.08	215.63	
$0.25\text{ Pt/g-C}_3N_4$	1009	5.10	253.68	2.0
$0.25\text{ Pt/6 T/g-C}_3N_4$	1195	5.03	519.73	

the most obvious for the  $TiO_2$ -noble metal co-modified one. From the electrochemical reduction tests and the photocatalytic activities for  $H_2$  evolution, one can see that the catalytic property and the visible-light activity for  $H_2$  evolution could be improved after decorating Au or Pt. The  $H_2$ -evolution activity is greatly improved after introducing  $TiO_2$  and decorating a noble metal, even much higher than the sum of  $6\text{ T/g-C}_3N_4$  and  $0.25\text{ metal/g-C}_3N_4$  samples (Table 1 and Fig. S12). This further demonstrates that it is much feasible to develop efficient photocatalysis for  $H_2$  evolution on  $g\text{-}C_3N_4$  by utilizing the synergistic effect confirmed above.

Particularly, one can notice that the visible-light photoactivities of metal-decorated  $g\text{-}C_3N_4$  for  $H_2$  evolution are improved after introducing a proper amount of anatase  $TiO_2$ , with different improvement times as follows (Table 1):  $4.6(\text{Ag}) > 2.7(\text{Au}) > 2.0(\text{Pt})$ , and it is much marked for the Ag-decorated one. Differently, it is generally acceptable, also according to the electrochemical reduction results (Fig. S12), that the catalytic functions for  $H_2$  evolution of decorated Ag, Au and Pt are gradually increased. Based on the TS-PL spectra (Figs. S10, S11, Tables S2, S3), it is confirmed that the decorated noble metal could easily accept the photogenerated electrons from  $g\text{-}C_3N_4$ , especially for the decorated Pt with the shorten TS-PL lifetime. However, the transferred electrons onto the decorated noble metal would quickly relax to the low Fermi energy level. Since the Fermi energy level of decorated noble metal is rather low, it is not feasible thermodynamically for the transferred electrons to induce the reduction reactions, consequently recombining with related holes. In this case, it is deduced that it is much beneficial for the decorated noble metal like Pt with good catalytic function to efficiently facilitate the transferred electrons with enough thermodynamic energy to initiate the reduction reactions. Thus, it is naturally understandable that it is much obvious for the confirmed synergistic effects of prolonging the charge lifetime and providing the catalytic function on efficient photocatalysis for  $H_2$  evolution in the g-

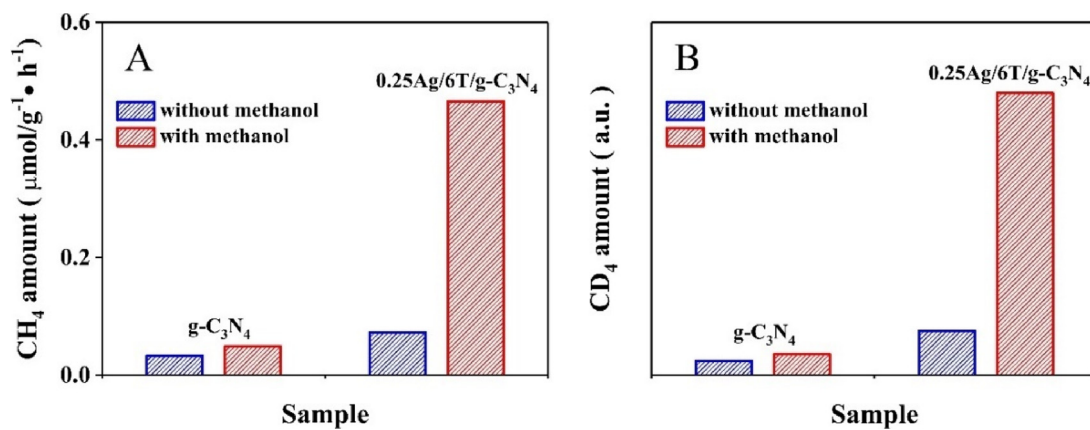
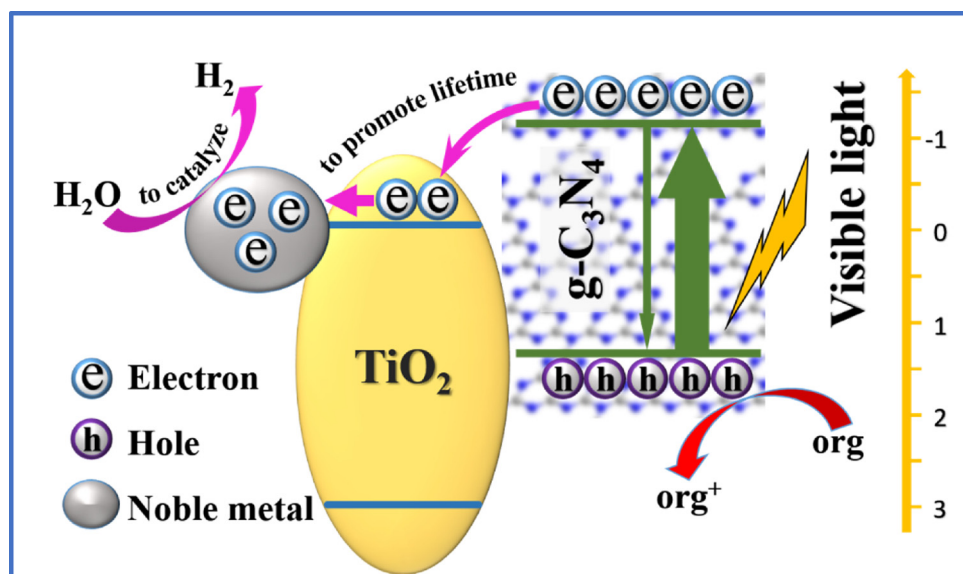


Fig. 5. Amounts of produced  $\text{CH}_4$  (A) and  $\text{CD}_4$  (B) from  $\text{CO}_2$  reduction respectively in  $\text{H}_2\text{O}$  and  $\text{D}_2\text{O}$  on  $\text{g-C}_3\text{N}_4$  and  $0.25\text{Ag}/6\text{T/g-C}_3\text{N}_4$  samples on the conditions of without and with methanol.



Scheme 1. Mechanism of the photogenerated charge transfer and induced photocatalytic processes for  $\text{H}_2$  evolution in the presence of methanol under visible-light irradiation on  $\text{g-C}_3\text{N}_4$  co-modified with noble metal and  $\text{TiO}_2$ .

$\text{C}_3\text{N}_4$  nanosheets co-modified with anatase  $\text{TiO}_2$  and noble metal with weak catalytic function like Ag. In other words, it is much necessary for the excited electrons with proper-energy to prolong the lifetime for effectively catalytic processes to produce  $\text{H}_2$ .

In addition, the above-confirmed synergistic effects are further supported by the similar co-modification with Ag and nanocrystalline  $\text{SnO}_2$ . As shown in the Fig. S13, it is shown from the XRD patterns and UV-vis DRS results that the  $0.25\text{Ag}/6\text{SnO}_2/\text{g-C}_3\text{N}_4$  sample is successfully synthesized [14,52]. According to the SS-SPS responses and the photocatalytic data, the observed results are similar to those of Ag and  $\text{TiO}_2$  co-modified  $\text{g-C}_3\text{N}_4$ . This well indicates that the coupled  $\text{SnO}_2$  could also act as the proper-energy platform to prolong the photogenerated charge lifetime, and then behave the synergistic effects with decorated Ag on efficient photocatalysis of  $\text{g-C}_3\text{N}_4$  for  $\text{H}_2$  evolution.

It is well established that methanol as an effective photogenerated hole capturer could be used to improve the photocatalytic activity for  $\text{H}_2$  evolution. Meanwhile, it also provides free  $\text{H}^+$ , which is favorable for electron-induced reduction reactions to produce  $\text{H}_2$  thermodynamically. In this case, it is expected that one evolved  $\text{H}_2$  is formed by two produced  $\cdot\text{H}$  radicals, and the produced  $\cdot\text{H}$  radicals mainly come from the reduction of  $\text{H}^+$  as a product of methanol oxidation other than from the adsorbed  $\text{H}_2\text{O}$ . To prove the expectation about the H resource of evolved  $\text{H}_2$  by photocatalysis, an isotope experiment of

photocatalytic  $\text{CO}_2$  reduction in  $\text{D}_2\text{O}$  has been designed to complete under the identical conditions since the produced  $\cdot\text{D}$  radicals would not enter into methane as the reduction production of  $\text{CO}_2$ . Gas chromatograph (GC) and gas chromatography-mass spectrometer (GC-MS) techniques were used to measure the amounts of  $\text{CH}_4$  in  $\text{H}_2\text{O}$  and of  $\text{CD}_4$  in  $\text{D}_2\text{O}$  (Fig. 5), respectively. One can see from Fig. 5A that the amounts of produced  $\text{CH}_4$  in  $\text{H}_2\text{O}$  on  $\text{g-C}_3\text{N}_4$  and  $0.25\text{Ag}/6\text{T/g-C}_3\text{N}_4$  are increased after adding methanol, respectively by  $\sim 1.48$  and  $\sim 6.38$  times. As shown in Figs. 5B and S14, the amounts of produced  $\text{CD}_4$  in  $\text{D}_2\text{O}$  on  $\text{g-C}_3\text{N}_4$  and  $0.25\text{Ag}/6\text{T/g-C}_3\text{N}_4$  are increased after adding methanol, respectively by  $\sim 1.44$  and  $\sim 6.36$  times. Unexpected, it is a surprisingly similar increase times of produced  $\text{CH}_4$  or  $\text{CD}_4$  amount on  $\text{g-C}_3\text{N}_4$  or on  $0.25\text{Ag}/6\text{T/g-C}_3\text{N}_4$  after adding methanol, strongly indicating that the H resource of evolved  $\text{H}_2$  by  $\text{g-C}_3\text{N}_4$  nanosheet-based photocatalysis is mainly from the adsorbed  $\text{H}_2\text{O}$  other than the  $\text{H}^+$  through methanol oxidation. Interestingly, this is in good agreement with the literature, in which it is confirmed by the mean of the called operando nuclear magnetic resonance spectra [53]. This is also supported by the FT-IR spectra (Fig. S15), by which it is confirmed that all resulting  $\text{g-C}_3\text{N}_4$ -based photocatalysts exhibit good capacity to adsorb  $\text{H}_2\text{O}$ . In addition, it is obvious for visible-light photocatalytic  $\text{CO}_2$  reduction to produce methane that the photoactivity of  $0.25\text{Ag}/6\text{T/g-C}_3\text{N}_4$  is much higher than that of  $\text{g-C}_3\text{N}_4$  by 2.2-time improvement

without methanol and by 9.5-time improvement with methanol.

On the basis of above results and discussion, a simple mechanism schematic is proposed as **Scheme 1**. Firstly, g-C<sub>3</sub>N<sub>4</sub> is excited by visible light to produce electron-hole pairs, and then the photogenerated holes are captured by CH<sub>3</sub>OH to initiate oxidation reactions. Meanwhile, the photogenerated electrons transfer from the CB of g-C<sub>3</sub>N<sub>4</sub> to the CB of TiO<sub>2</sub>, leading to the lifetime increase of photogenerated electrons with proper thermodynamic energy. Subsequently, the transferred electrons further move onto the decorated noble metal, at which the induced reduction reactions with the adsorbed H<sub>2</sub>O for H<sub>2</sub> evolution are catalyzed.

#### 4. Conclusions

In summary, the photocatalytic activities of g-C<sub>3</sub>N<sub>4</sub> nanosheets for H<sub>2</sub> evolution under visible-light irradiation have been greatly improved after coupling TiO<sub>2</sub> and then decorating a noble metal. The improved activity is attributed to the synergistic effect of prolonging the charge lifetime and catalyzing H<sub>2</sub> evolution. The prolonged charge lifetime is originated from the coupled TiO<sub>2</sub> for it could act as a proper-energy platform for accepting visible-light-excited electrons from g-C<sub>3</sub>N<sub>4</sub>. The catalyzing capability is originated from the decorated noble metal for it could act as the co-catalyst for H<sub>2</sub> evolution. Moreover, it is much necessary for the used noble metal cocatalyst with weak catalytic function like Ag for H<sub>2</sub> evolution to prolong the photogenerated charge lifetime. Moreover, it is clearly confirmed that the evolved H<sub>2</sub> mainly originates from the adsorbed water other than the disassociated H<sup>+</sup> from methanol. This work provides new physical insights and feasible routes to develop efficient g-C<sub>3</sub>N<sub>4</sub>-based photocatalysts for energy production, and the confirmed synergistic effect is also applicable to other narrow-bandgap photocatalysts.

#### Acknowledgements

We are grateful to financial support from NSFC (U1401245, 21501052, 91622119), the Program for Innovative Research Team in Chinese Universities (IRT1237) and the Research Project of Chinese Ministry of Education (213011A).

#### Appendix A. Supplementary data

Supplementary material related to this article can be found, in the online version, at doi:<https://doi.org/10.1016/j.apcatb.2018.05.034>.

#### References

- [1] E. Alberico, P. Sponholz, C. Cordes, M. Nielsen, H. Drexler, W. Baumann, H. Junge, M. Beller, Selective hydrogen production from methanol with a defined iron pincer catalyst under mild conditions, *Angew. Chem. Int. Ed.* 52 (2013) 14162–14166.
- [2] A. Hafizi, M.R. Rahimpour, S. Hassanajili, Hydrogen production via chemical looping steam methane reforming process: effect of cerium and calcium promoters on the performance of Fe<sub>2</sub>O<sub>3</sub>/Al<sub>2</sub>O<sub>3</sub> oxygen carrier, *Appl. Energy* 165 (2016) 685–694.
- [3] M.Y. Liu, W. Zhou, T. Wang, D.F. Wang, L.Q. Liu, J.H. Ye, High performance Au–Cu alloy for enhanced visible-light water splitting driven by coinage metals, *Chem. Commun.* 52 (2016) 4694–4697.
- [4] D. Chen, H. Zhang, Y. Liu, J. Li, Graphene and its derivatives for the development of solar cells, photoelectrochemical, and photocatalytic applications, *Energ. Environ. Sci.* 6 (2013) 1362.
- [5] C. Jiang, S.J.A. Moniz, A. Wang, T. Zhang, J. Tang, Photoelectrochemical devices for solar water splitting - materials and challenges, *Chem. Soc. Rev.* 46 (2017) 4645–4660.
- [6] J. Li, H. Li, G. Zhan, L. Zhang, Solar water splitting and nitrogen fixation with layered bismuth oxyhalides, *Acc. Chem. Res.* 50 (2017) 112–121.
- [7] C. Yang, J. Qin, Z. Xue, M. Ma, X. Zhang, R. Liu, Rational design of carbon-doped TiO<sub>2</sub> modified g-C<sub>3</sub>N<sub>4</sub> via in-situ heat treatment for drastically improved photocatalytic hydrogen with excellent photostability, *Nano Energy* 41 (2017) 1–9.
- [8] W. He, Y. Yang, L. Wang, J. Yang, X. Xiang, D. Yan, F. Li, Photoelectrochemical water oxidation efficiency of a core/shell array photoanode enhanced by a dual suppression strategy, *ChemSusChem* 8 (2015) 1568–1576.
- [9] L. Yao, N. Zhang, Y. Wang, Y. Ni, D. Yan, C. Hu, Facile formation of 2D Co<sub>2</sub>P@Co<sub>3</sub>O<sub>4</sub> microsheets through in-situ topochemical conversion and surface corrosion: bifunctional electrocatalysts towards overall water splitting, *J. Power Sources* 374 (2018) 142–148.
- [10] F. Raziq, L. Sun, Y. Wang, X. Zhang, M. Humayun, S. Ali, L. Bai, Y. Qu, H. Yu, L. Jing, Synthesis of large surface-area g-C<sub>3</sub>N<sub>4</sub> comodified with MnO<sub>x</sub> and Au-TiO<sub>2</sub> as efficient visible-light photocatalysts for fuel production, *Adv. Energy Mater.* 8 (2018) 1701580.
- [11] X. She, J. Wu, J. Zhong, H. Xu, Y. Yang, R. Vajtai, J. Lou, Y. Liu, D. Du, H. Li, P.M. Ajayan, Oxygenated monolayer carbon nitride for excellent photocatalytic hydrogen evolution and external quantum efficiency, *Nano Energy* 27 (2016) 138–146.
- [12] L.H. Yao, D. Wei, Y.M. Ni, D.P. Yan, C.W. Hu, Surface localization of CdZnS quantum dots onto 2D g-C<sub>3</sub>N<sub>4</sub> ultrathin microribbons: highly efficient visible light-induced H<sub>2</sub>-generation, *Nano Energy* 26 (2016) 248–256.
- [13] Y. Zheng, L.H. Lin, X.J. Ye, F.S. Guo, X.C. Wang, Helical graphitic carbon nitrides with photocatalytic and optical activities, *Angew. Chem. Int. Ed.* 53 (2014) 11926–11930.
- [14] A. Zada, M. Humayun, F. Raziq, X. Zhang, Y. Qu, L. Bai, C. Qin, L. Jing, H. Fu, exceptional visible-light-driven cocatalyst-free photocatalytic activity of g-C<sub>3</sub>N<sub>4</sub> by well designed nanocomposites with plasmonic Au and SnO<sub>2</sub>, *Adv. Energy Mater.* 6 (2016) 1601190.
- [15] J. Zhang, M. Zhang, C. Yang, X. Wang, Nanospherical carbon nitride frameworks with sharp edges accelerating charge collection and separation at a soft photocatalytic interface, *Adv. Mater.* 26 (2014) 4121–4126.
- [16] H. Shi, G. Chen, C. Zhang, Z. Zou, Polymeric g-C<sub>3</sub>N<sub>4</sub> coupled with NaNbO<sub>3</sub> nanowires toward enhanced photocatalytic reduction of CO<sub>2</sub> into renewable fuel, *ACS Catal.* 4 (2014) 3637–3643.
- [17] X.D. Li, Y. Feng, M.C. Li, W. Li, H. Wei, D.D. Song, Smart hybrids of Zn<sub>2</sub>GeO<sub>4</sub> nanoparticles and ultrathin g-C<sub>3</sub>N<sub>4</sub> layers: synergistic lithium storage and excellent electrochemical performance, *Adv. Funct. Mater.* 25 (2015) 6858–6866.
- [18] S. Obregon, G. Colon, Improved H<sub>2</sub> production of Pt-TiO<sub>2</sub>/g-C<sub>3</sub>N<sub>4</sub>-MnO<sub>x</sub> composites by an efficient handling of photogenerated charge pairs, *Appl. Catal., B-Environ.* 144 (2014) 775–782.
- [19] Y.M. He, Y. Wang, L.H. Zhang, B.T. Teng, M.H. Fan, High-efficiency conversion of CO<sub>2</sub> to fuel over ZnO/g-C<sub>3</sub>N<sub>4</sub> photocatalyst, *Appl. Catal. B Environ.* 168 (2015) 1–8.
- [20] Y.P. Zang, L.P. Li, Y.S. Xu, Y. Zuo, G.S. Li, Hybridization of brookite TiO<sub>2</sub> with g-C<sub>3</sub>N<sub>4</sub>: a visible-light-driven photocatalyst for As<sup>3+</sup> oxidation, MO degradation and water splitting for hydrogen evolution, *J. Mater. Chem. A* 2 (2014) 15774–15780.
- [21] M.J. Munoz-Batista, O. Fontelles-Carceler, M. Ferrer, M. Fernandez-Garcia, A. Kubacka, Disinfection capability of Ag/g-C<sub>3</sub>N<sub>4</sub> composite photocatalysts under UV and visible light illumination, *Appl. Catal. B Environ.* 183 (2016) 86–95.
- [22] G.F. Long, X.H. Li, K. Wan, Z.X. Liang, J.H. Piao, P. Tsikaras, Pt/CN-doped electrocatalysts: superior electrocatalytic activity for methanol oxidation reaction and mechanistic insight into interfacial enhancement, *Appl. Catal. B Environ.* 203 (2017) 541–548.
- [23] X.B. Wei, C.L. Shao, X.H. Li, N. Lu, K.X. Wang, Z.Y. Zhang, Y.C. Liu, Facile in situ synthesis of plasmonic nanoparticles-decorated g-C<sub>3</sub>N<sub>4</sub>/TiO<sub>2</sub> heterojunction nanofibers and comparison study of their photo synergistic effects for efficient photocatalytic H<sub>2</sub> evolution, *Nanoscale* 8 (2016) 11034–11043.
- [24] H.F. Li, H.T. Yu, X. Quan, S. Chen, Y.B. Zhang, Uncovering the key role of the fermi level of the electron mediator in a Z-scheme photocatalyst by detecting the charge transfer process of WO<sub>3</sub>-metal-g-C<sub>3</sub>N<sub>4</sub> (metal = Cu, Ag, Au), *ACS App. Mater. Inter.* 8 (2016) 2111–2119.
- [25] M. Xie, X. Fu, L. Jing, P. Luan, Y. Feng, H. Fu, Long-lived, visible-light-excited charge carriers of TiO<sub>2</sub>/BiVO<sub>4</sub> nanocomposites and their unexpected photoactivity for water splitting, *Adv. Energy Mater.* 4 (2014) 1300995.
- [26] G.M. Haselmann, D. Eder, Early-stage deactivation of platinum-loaded TiO<sub>2</sub> using in situ photodeposition during photocatalytic hydrogen evolution, *ACS Catal.* 7 (2017) 4668–4675.
- [27] H. He, J. Lin, W. Fu, X. Wang, H. Wang, Q. Zeng, Q. Gu, Y. Li, C. Yan, B.K. Tay, C. Xue, X. Hu, S.T. Pantelides, W. Zhou, Z. Liu, MoS<sub>2</sub>/TiO<sub>2</sub> edge-on heterostructure for efficient photocatalytic hydrogen evolution, *Adv. Energy Mater.* 6 (2016) 1600464.
- [28] V.M. Friebe, J.D. Delgado, D.J.K. Swainsbury, J.M. Gruber, A. Chanaewa, R. van Grondelle, E. von Hauff, D. Millo, M.R. Jones, R.N. Frese, Plasmon-enhanced photocurrent of photosynthetic pigment proteins on nanoporous silver, *Adv. Funct. Mater.* 26 (2016) 285–292.
- [29] Y. Choi, H. Kim, G. Moon, S. Jo, W. Choi, Boosting up the low catalytic activity of silver for H<sub>2</sub> production on Ag/TiO<sub>2</sub> photocatalyst: thiocyanate as a selective modifier, *ACS Catal.* 6 (2016) 821–828.
- [30] F.Y. Zhang, B. Yang, X. Mao, R.X. Yang, L. Jiang, Y.J. Li, J. Xiong, Y. Yang, R.X. He, W.Q. Deng, K.L. Han, Perovskite CH<sub>3</sub>NH<sub>3</sub>PbI<sub>3</sub>-xBr<sub>x</sub> single crystals with charge-carrier lifetimes exceeding 260 μs, *ACS App. Mater. Inter.* 9 (2017) 14827–14832.
- [31] M.Y. Zhu, Q. Liu, W. Chen, Y.Y. Yin, L. Ge, H.N. Li, K. Wane, Boosting the visible-light photoactivity of BiOCl/BiVO<sub>4</sub>/N-GQD ternary heterojunctions based on internal z-scheme charge transfer of N-GQDs: simultaneous band gap narrowing and carrier lifetime prolonging, *ACS App. Mater. Inter.* 9 (2017) 38832–38841.
- [32] J.N. Schrauben, R. Hayoun, C.N. Valdez, M. Braten, L. Fridley, J.M. Mayer, Titanium and zinc oxide nanoparticles are proton-coupled electron transfer agents, *Science* 336 (2012) 1298–1301.
- [33] C. Xu, W. Yang, Q. Guo, D. Dai, M. Chen, X. Yang, Molecular hydrogen formation from photocatalysis of methanol on TiO<sub>2</sub>(110), *J. Am. Chem. Soc.* 135 (2013) 10206–10209.
- [34] V.M. Sanchez, J.A. Cojulun, D.A. Scherlis, Dissociation free energy profiles for water and methanol on TiO<sub>2</sub> surfaces, *J. Phys. Chem. C* 114 (2010) 11522–11526.
- [35] T. Chen, Z.H. Feng, G.P. Wu, J.Y. Shi, G.J. Ma, P.L. Ying, C. Li, Mechanistic studies

- of photocatalytic reaction of methanol for hydrogen production on Pt/TiO<sub>2</sub> by in situ fourier transform IR and time-resolved IR spectroscopy, *J. Phys. Chem. C* 111 (2007) 8005–8014.
- [36] P. Niu, Y.Q. Yang, J.C. Yu, G. Liu, H.M. Cheng, Switching the selectivity of the photoreduction reaction of carbon dioxide by controlling the band structure of a g-C<sub>3</sub>N<sub>4</sub> photocatalyst, *Chem. Commun.* 50 (2014) 10837–10840.
- [37] Y.B. Luan, L.Q. Jing, Y. Xie, X.J. Sun, Y.J. Feng, H.G. Fu, Exceptional photocatalytic activity of 001-facet-exposed TiO<sub>2</sub> mainly depending on enhanced adsorbed oxygen by residual hydrogen fluoride, *ACS Catal.* 3 (2013) 1378–1385.
- [38] Z. Zhu, Z.Y. Lu, D.D. Wang, X. Tang, Y.S. Yan, W.D. Shi, Y.S. Wang, N.L. Gao, X. Yao, H.J. Dong, Construction of high-dispersed Ag/Fe<sub>3</sub>O<sub>4</sub>/g-C<sub>3</sub>N<sub>4</sub> photocatalyst by selective photo-deposition and improved photocatalytic activity, *Appl. Catal. B Environ.* 182 (2016) 115–122.
- [39] S. Ma, S. Zhan, Y. Jia, Q. Shi, Q. Zhou, Enhanced disinfection application of Ag-modified g-C<sub>3</sub>N<sub>4</sub> composite under visible light, *Appl. Catal. B Environ.* 186 (2016) 77–87.
- [40] D.J. Martin, K.P. Qiu, S.A. Shevlin, A.D. Handoko, X.W. Chen, Z.X. Guo, J.W. Tang, Highly efficient photocatalytic H<sub>2</sub> evolution from water using visible light and structure-controlled graphitic carbon nitride, *Angew. Chem. Int. Ed.* 53 (2014) 9240–9245.
- [41] Y.F. Chen, W.X. Huang, D.L. He, S.T. Yue, H. Huang, Construction of hetero-structured g-C<sub>3</sub>N<sub>4</sub>/Ag/TiO<sub>2</sub> microspheres with enhanced photocatalysis performance under visible-light irradiation, *ACS Appl. Mater. Inter.* 6 (2014) 14405–14414.
- [42] H.L. Hou, F.M. Gao, L. Wang, M.H. Shang, Z.B. Yang, J.J. Zheng, W.Y. Yang, Superior thoroughly mesoporous ternary hybrid photocatalysts of TiO<sub>2</sub>/WO<sub>3</sub>/g-C<sub>3</sub>N<sub>4</sub> nanofibers for visible-light-driven hydrogen evolution, *J. Mater. Chem. A* 4 (2016) 6276–6281.
- [43] X. Xin, J.Y. Lang, T.T. Wang, Y.G. Su, Y.X. Zhao, X.J. Wang, Construction of novel ternary component photocatalyst Sr<sub>0.25</sub>H<sub>1.5</sub>Ta<sub>2</sub>O<sub>6</sub> center dot H<sub>2</sub>O coupled with g-C<sub>3</sub>N<sub>4</sub> and Ag toward efficient visible light photocatalytic activity for environmental remediation, *Appl. Catal. B Environ.* 181 (2016) 197–209.
- [44] X.Y. Pan, X.X. Chen, Z.G. Yi, Defective porous TiO<sub>2</sub> nanosheets with Pt decoration as an efficient photocatalyst for ethylene oxidation synthesized by a C<sub>3</sub>N<sub>4</sub> templating method, *ACS Appl. Mater. Inter.* 8 (2016) 10104–10108.
- [45] Y. Luan, L. Jing, M. Xie, X. Shi, X. Fan, Y. Cao, Y. Feng, Synthesis of efficient N-containing TiO<sub>2</sub> photocatalysts with high anatase thermal stability and the effects of the nitrogen residue on the photoinduced charge separation, *Phys. Chem. Chem. Phys.* 14 (2012) 1352–1359.
- [46] H.J. Queisser, D.E. Theodorou, Decay kinetics of persistent photoconductivity in semiconductors, *Phys. Rev. B* 33 (1986) 4027–4033.
- [47] R. Godin, Y. Wang, M.A. Zwijnenburg, J. Tang, J.R. Durrant, Time-resolved spectroscopic investigation of charge trapping in carbon nitrides photocatalysts for hydrogen generation, *J. Am. Chem. Soc.* 139 (2017) 5216–5224.
- [48] Y. Nakabayashi, Y. Nosaka, OH radical formation at distinct faces of rutile TiO<sub>2</sub> crystal in the procedure of photoelectrochemical water oxidation, *J. Phys. Chem. C* 117 (2013) 23832–23839.
- [49] T. Bhowmik, M.K. Kundu, S. Barman, Palladium nanoparticle-graphitic carbon nitride porous synergistic catalyst for hydrogen evolution/oxidation reactions over a broad range of pH and correlation of its catalytic activity with measured hydrogen binding energy, *ACS Catal.* 6 (2016) 1929–1941.
- [50] Y. Tang, X. Fang, X. Zhang, G. Fernandes, Y. Yan, D. Yan, X. Xiang, J. He, Space-confined earth-abundant bifunctional electrocatalyst for high-efficiency water splitting, *ACS Appl. Mater. Inter.* 9 (2017) 36762–36771.
- [51] B.B. Xie, Y. Zhang, N. Du, H.P. Li, W.G. Hou, R.J. Zhang, Preparation of preferentially exposed poison-resistant Pt(111) nanoplates with a nitrogen-doped graphene aerogel, *Chem. Commun.* 52 (2016) 13815–13818.
- [52] Z. Li, P. Luan, X. Zhang, Y. Qu, F. Raziq, J. Wang, L. Jing, Prolonged lifetime and enhanced separation of photogenerated charges of nanosized  $\alpha$ -Fe<sub>2</sub>O<sub>3</sub> by coupling SnO<sub>2</sub> for efficient visible-light photocatalysis to convert CO<sub>2</sub> and degrade acet-aldehyde, *Nano Res.* 10 (2017) 2321–2331.
- [53] X.L. Wang, W. Liu, Y.Y. Yu, Y. Song, W.Q. Fang, D. Wei, X.Q. Gong, Y.F. Yao, H.G. Yang, Operando NMR spectroscopic analysis of proton transfer in heterogeneous photocatalytic reactions, *Nat. Commun.* 7 (2016) 11918.